JOURNAL OF GEOPHYSICAL RESEARCH, VOL. 112, B08201, doi:10.1029/2006JB004511, 2007

ENTERED

Click Here for Full Article

The $^{40}Ar/^{39}Ar$ age constraints on the duration of resurgence at the Valles caldera, New Mexico

Erin H. Phillips,[1] Fraser Goff,[2] Philip R. Kyle,[1,3] William C. McIntosh,[1,3] Nelia W. Dunbar,[3] and Jamie N. Gardner[4]

Received 17 May 2006; revised 25 February 2007; accepted 3 April 2007; [redacted]

[1] The $^{40}Ar/^{39}Ar$ ages for rocks from the Valles caldera, New Mexico, imply that resurgent uplift of the caldera floor occurred within 27 ± 27 ka of caldera collapse. The structural resurgent dome of the Valles caldera was uplifted approximately 1000 m above the surrounding caldera floor during resurgence. The upper Bandelier Tuff, which yields an age of 1.256 ± 0.010 Ma (2σ; ages relative to Fish Canyon tuff sanidine at 28.02 Ma), is the lower constraint on the timing of resurgence. The oldest postcollapse ring fracture dome, Cerro del Medio, is the upper time constraint and yields an age of 1.229 ± 0.017 Ma for one of its oldest flow lobes. Therefore resurgent uplift probably occurred within 54 ka, at a minimum rate of 1.9 cm/yr. Sanidine phenocrysts from rhyolites of the postcollapse intracaldera Deer Canyon and Redondo Creek members yield $^{40}Ar/^{39}Ar$ single-crystal laser fusion ages ranging from 1.229 ± 0.013 Ma to 1.283 ± 0.017 Ma (Deer Canyon Member; n = 8) and 1.208 ± 0.017 Ma to 1.239 ± 0.017 Ma (Redondo Creek Member; n = 4). With one exception from each unit, these ages are statistically indistinguishable from the upper Bandelier Tuff, indicating that eruption of these postcollapse rhyolites probably commenced shortly after caldera formation. Melt inclusion hosted excess argon was not found to have a measurable effect on the age of sanidine from the upper Bandelier Tuff or the Deer Canyon Member.

Citation: Phillips, E. H., F. Goff, P. R. Kyle, W. C. McIntosh, N. W. Dunbar, and J. N. Gardner (2007), The $^{40}Ar/^{39}Ar$ age constraints on the duration of resurgence at the Valles caldera, New Mexico, *J. Geophys. Res.*, *112*, B08201, doi:10.1029/2006JB004511.

1. Introduction

[2] The collapse of large ignimbrite forming calderas is often followed by uplift of the caldera floor to form a central structural dome, a process known as resurgence [*Smith and Bailey*, 1968]. Caldera resurgence can cause considerable uplift. At the Valles caldera in New Mexico, the resurgent dome rises over 1000 m above the surrounding caldera floor [*Smith and Bailey*, 1968]. An understanding of the timing and rates of resurgence is of interest not only for the study of previously active calderas, such as the Valles caldera, but for volcanic centers that have experienced more recent uplift, such as Yellowstone, Long Valley, Campi Flegrei, and Iwo-Jima [e.g., *Jackson et al.*, 1984; *Kaizuka et al.*, 1989; *Luongo et al.*, 1991; *Sorey et al.*, 2003].

[3] The Valles caldera in the Jemez Mountains of New Mexico is the type example of a resurgent caldera [*Smith and Bailey*, 1968]. Because of its young age (1.25 Ma) and location in a relatively dry climate, it is well preserved and yields important details about the nature and timing of resurgence. Eruption of the upper Bandelier Tuff occurred concurrently with the collapse of the Valles caldera and resulted in the deposition of approximately 250 km^3 of rhyolitic ignimbrite and 15 km^3 (dense rock equivalent) of precursor Plinian fall deposits [*Self et al.*, 1996]. The Valles caldera exhibits a distinct geometry in which the resurgent dome lies near what was once the center of the collapsed caldera. Intracaldera geologic relations on and near the resurgent dome are complex, reflecting the chaotic nature of the events that occurred after collapse [*Goff et al.*, 2006a]. Postcollapse intracaldera volcanism resulted in eruption of the Deer Canyon and Redondo Creek members of the Valles Rhyolite Formation, which are intricately interlayered with caldera fill sediments. Megabreccia blocks composed of precaldera lithologies are found intermixed with intracaldera upper Bandelier Tuff [*Phillips*, 2004]. Postcollapse ring fracture domes reveal the location of the caldera's structural perimeter [*Smith and Bailey*, 1968].

[4] The primary purpose of this study is to better understand the timing and duration of resurgence. The $^{40}Ar/^{39}Ar$ dating method affords many advantages for dating Quaternary volcanic rocks, including a high level of precision. This is important when attempting to resolve the ages of rocks erupted within a relatively short period (<100 ka).

[1]Department of Earth and Environmental Science, New Mexico Institute of Mining and Technology, Socorro, New Mexico, USA.
[2]Department of Earth and Planetary Sciences, University of New Mexico, Albuquerque, New Mexico, USA.
[3]New Mexico Bureau of Geology and Mineral Resources, New Mexico Institute of Mining and Technology, Socorro, New Mexico, USA.
[4]Earth and Environmental Sciences Division, Los Alamos National Laboratory, Los Alamos, New Mexico, USA.

Copyright 2007 by the American Geophysical Union.
0148-0227/07/2006JB004511$09.00

34101

Single-crystal laser fusion allows for the identification of xenocrysts and crystals with anomalous ages, which are common in rhyolitic ignimbrites. In this study, ^{40}Ar/^{39}Ar geochronology is used (1) to determine the ages of the postcollapse intracaldera Deer Canyon and Redondo Creek members and (2) to date the upper Bandelier Tuff and Cerro del Medio, the oldest postcollapse ring fracture dome, to provide time constraints on resurgence. Establishing age constraints on the duration of resurgence provides information about the timing and rate of resurgent uplift. These findings are then used to examine the physicomagmatic nature of resurgence at the Valles caldera, to confirm that resurgence commenced very soon after caldera collapse, and to compare and contrast the Valles caldera with other resurgent caldera systems.

2. Volcanism in the Jemez Mountains

[5] The Valles caldera is located in the Jemez Mountains in north central New Mexico and is part of the Jemez Volcanic Field (Figure 1). It is situated at the intersection of the Rio Grande rift and the Jemez Lineament. The Rio Grande rift is a major Cenozoic extensional feature that extends from Colorado to Mexico [*Chapin and Seager*, 1975; *Baldridge et al.*, 1980; *Seager et al.*, 1984; *Olsen et al.*, 1987]. The Jemez Lineament is a northeast-southwest trending zone of concentrated tectonic activity that has been volcanically active from Miocene to Quaternary time [*Baldridge et al.*, 1983; *Olsen et al.*, 1987].

[6] Volcanism in the Jemez Mountains commenced at ~16.5 Ma [*Gardner and Goff*, 1984; *Gardner et al.*, 1986; *Goff and Gardner*, 2004]. The stratigraphic relations in the Jemez Volcanic Field were described by *Bailey et al.* [1969] and *Smith et al.* [1970] and later refined by *Gardner et al.* [1986] and *Self et al.* [1986]. The Bandelier Tuff and units associated with the collapse and resurgence of the Valles caldera, which are the focus of this study, are part of the Tewa Group, which includes rocks between approximately 1.85 Ma and 0.04 Ma [*Spell et al.*, 1996; *Goff and Gardner*, 2004]. The Bandelier Tuff Formation is divided into the Tshirege Member and the Otowi Member, which are referred to here by their informal names, the upper Bandelier Tuff (UBT) and the lower Bandelier Tuff (LBT), respectively.

[7] The LBT erupted at ~1.6 Ma, concurrently with the collapse of the Toledo caldera [*Izett and Obradovich*, 1994; *Spell et al.*, 1996]. The eruption of the UBT and collapse of the Valles caldera occurred at ~1.25 Ma. The Valles caldera and the Toledo caldera probably shared the same location, and the ring fracture of the Valles caldera lies within the slightly larger ring fracture of the Toledo Caldera [*Heiken et al.*, 1986; *Self et al.*, 1986]. The Cerro Toledo Rhyolite formed a group of domes and tephra between the two caldera forming eruptions [*Stix et al.*, 1988; *Spell et al.*, 1996].

[8] Following collapse of the Valles caldera, resurgent uplift of the caldera floor occurred, which formed a central structural dome. This resurgent dome, known as Redondo Peak, rises over 1000 m above the surrounding caldera floor (Figure 1). *Smith and Bailey* [1968] described the Valles caldera and proposed a seven-stage model for the formation of resurgent calderas. In this model, resurgence follows caldera collapse and ignimbrite eruption, and therefore the age of the UBT is an appropriate lower constraint on the timing of resurgence.

[9] The oldest Valles Rhyolite Formation eruptions were of the Deer Canyon and Redondo Creek members, which overlie intracaldera UBT [*Smith and Bailey*, 1968; *Bailey et al.*, 1969; *Smith et al.*, 1970] (Figure 1). Stratigraphic relationships show that at least some Deer Canyon Member eruptions predate the Redondo Creek Member [*Smith et al.*, 1970]. The Deer Canyon Member includes rhyolitic lavas, lithic tuffs, and breccias. Sanidine and quartz are the most abundant phenocryst phases. The "Upper Tuffs" unit described by *Nielson and Hulen* [1984] from wells drilled on the resurgent dome consists of tuffs of the Deer Canyon Member. The Redondo Creek Member consists primarily of rhyolitic lavas and is unique among intracaldera units because of its lack of quartz. Intracaldera stratigraphy is complex and the Deer Canyon and Redondo Creek members are found interlayered with caldera fill sediments, which include debris flows and finer sedimentary material of fluvial and lacustrine origin [*Goff et al.*, 2006a; *Chipera et al.*, 2007].

[10] Megabreccia blocks of the type described by *Lipman* [1976] are intermixed with UBT inside the Valles caldera (Figure 1). The ^{40}Ar/^{39}Ar ages for selected megabreccia blocks are given by *Phillips et al.* [2007].

[11] Ring fracture rhyolite domes of the Valle Grande Member of the Valles Rhyolite Formation encircle the structural resurgent dome of the Valles caldera (Figure 1). They were erupted between ~1.2 and 0.5 Ma [*Spell and Harrison*, 1993; *Singer and Brown*, 2002]. Cerro del Medio, the oldest ring fracture dome, is a dome and flow complex with six distinctive effusive and at least two pyroclastic eruptive phases [*Gardner et al.*, 2006]. There is no apparent tilting, faulting, or deformation of Cerro del Medio due to resurgent uplift, although the base of the unit is not exposed. The western edge of Cerro del Medio is less than 500 m from the resurgent dome, where major graben faults exhibit at least 300 m of displacement and show intense alteration [*Smith et al.*, 1970; *Phillips*, 2004; *Goff et al.*, 2006a]. This supports the premise that resurgent uplift was complete before the emplacement of Cerro del Medio. It is therefore our contention that the ages of the oldest flow lobes of Cerro del Medio provide an appropriate upper constraint on the timing of resurgence.

3. The ^{40}Ar/^{39}Ar Methods

[12] Rocks selected for ^{40}Ar/^{39}Ar dating consisted of four UBT, eight Deer Canyon Member, four Redondo Creek Member, and two Cerro del Medio samples. All samples, with the exception of two UBT samples, were collected within the Valles caldera (Figure 1). Where possible, samples were collected from outcrops with little or no alteration. However, due to the extensive intracaldera hydrothermal alteration and limited outcrop, some rocks with slight hydrothermal alteration were sampled. In most samples, phenocrysts were unaltered. For samples in which slight alteration was present, including those from Cerro del Medio, care was taken to hand-pick the most pristine crystals for ^{40}Ar/^{39}Ar analysis.

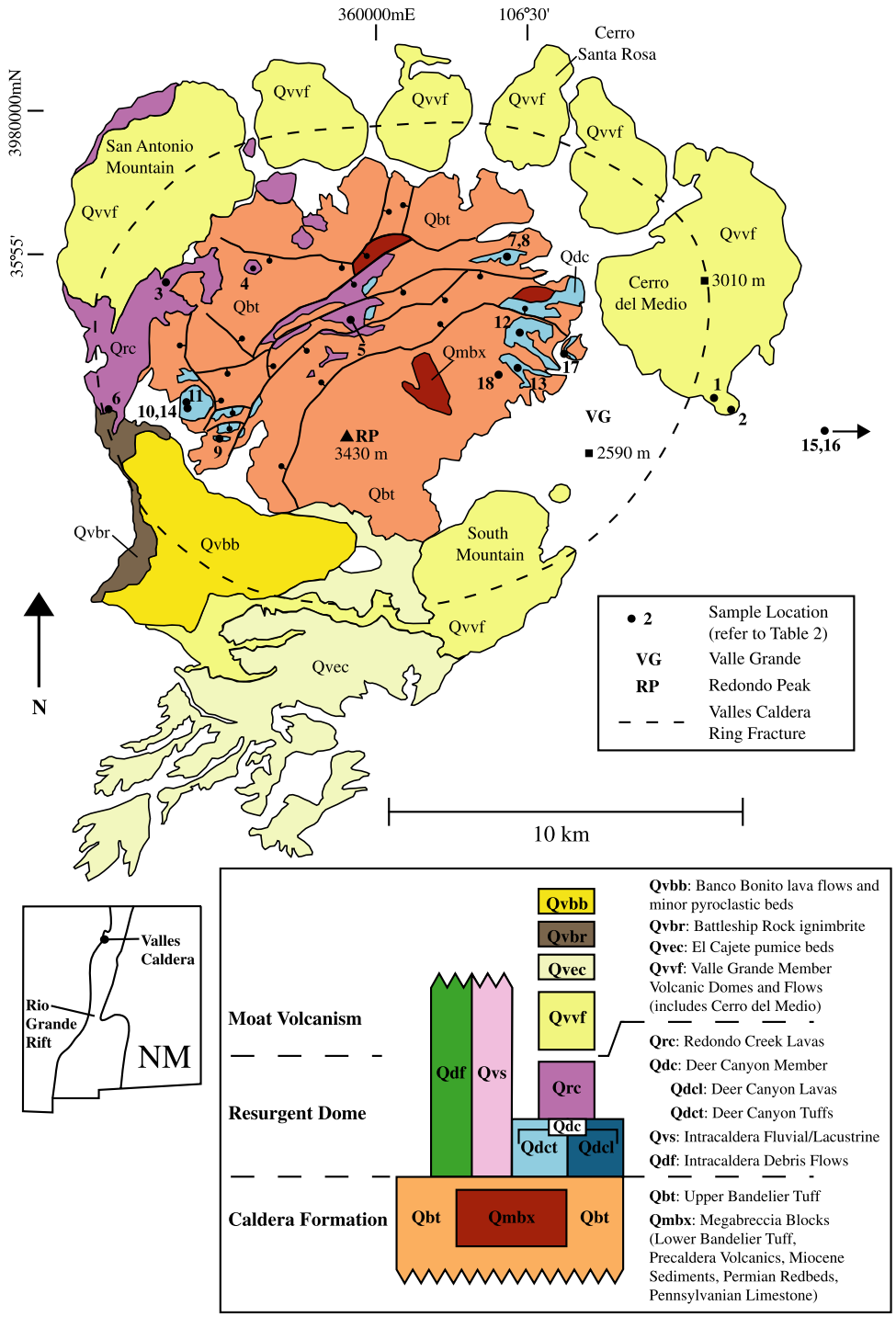

Figure 1. Generalized map and stratigraphy of the Valles caldera modified from *Smith et al.* [1970]. Map includes Redondo Creek rhyolite and selected large megabreccia blocks mapped by *Goff et al.* [2005, 2006a, 2006b; *Gardner et al.*, 2006]. Refer to Table 2 for sample locations. Caldera fill units (Qdf, Qvs) are not shown for clarity. Spot elevations are shown for reference. Deer Canyon tuffs and lavas are undivided. Sample points 15 and 16 are the Plinian fall deposit and outflow facies upper Bandelier Tuff, respectively, that were sampled east of the caldera.

[13] Rock samples were crushed and sieved to obtain the optimal size fraction for mineral separation (typically 425–850 μm). Sanidine was separated by standard magnetic, heavy liquid, and hand-picking techniques, and etched for 5–20 min in 15% hydrofluoric acid (HF).

[14] A Cameca SX-100 electron microprobe was used to characterize the texture and chemistry of mineral separates for ^{40}Ar/^{39}Ar analysis and to assess the abundance and character of melt inclusions for the study of excess argon. The microprobe was particularly useful for identifying

Table 1. Irradiation Data, Correction Factors, Discrimination Values, and Mass Spectrometer Sensitivity for Irradiations NM-160, NM-165, and NM-172[a]

	Irradiation NM-160[b]	Irradiation NM-165	Irradiation NM-172
Reactor facility	Texas A&M University Research Reactor[c]	Ford Memorial Reactor, University of Michigan[d]	Texas A&M University Research Reactor[c]
Correction factors[e]			
$(^{36}Ar/^{37}Ar)_{Ca}$	0.00028 ± 0.000005	0.00028 ± 0.00001	0.00028 ± 0.000005
$(^{39}Ar/^{37}Ar)_{Ca}$	0.0007 ± 0.00002	0.00075 ± 0.00005	0.0007 ± 0.00002
$(^{40}Ar/^{39}Ar)_{K}$	0.0002 ± 0.0003	0.0232 ± 0.0009	0.0002 ± 0.0003
Discrimination[f]	1.00520 ± 0.00172, 1.00737 ± 0.00192, 1.00743 ± 0.00124	1.00484 ± 0.00092 and 1.00562 ± 0.00081	1.005 ± 0.001
Mass spectrometer sensitivity, mol/pA	1.41×10^{-16} (laser)	1.56×10^{-16} (laser); 2.82×10^{-16} (furnace)	1.46×10^{-16} (laser)

[a]Samples and neutron flux monitors were placed in machined aluminum disks for irradiation. Crystals were loaded in holes of a known geometry in the disks, which were stacked vertically and sealed in a Pyrex tube (NM-160, NM-172) or a quartz tube (NM-165).
[b]Samples and monitors from irradiation NM-160 were analyzed during two different time intervals, resulting in two different J factors for some samples. The two J factors were not averaged because of possible variations in the actual discrimination values.
[c]Irradiated for 7 hours in the D3 position.
[d]Irradiated for 9.9 hours in the L-67 position.
[e]Determined by analysis of CaF_2 and K glass.
[f]Samples were analyzed over a period of approximately 2 years, during which time discrimination values were assessed periodically.

samples containing altered sanidine crystals or crystals that exhibited xenocrystic features such as a compositionally mottled texture [*Phillips*, 2004]. For quantitative analysis of feldspars, count times of 20 seconds were used for Na, K, Ca, and errors for those elements were based on replicate analysis of feldspar reference material [*Phillips et al.*, 2007].

[15] Samples and neutron flux monitors were irradiated in packages NM-160, NM-165, and NM-172. NM-165 included crushed and etched sanidine samples used to evaluate excess argon. This package was not shielded for thermal neutrons, which allows for the laboratory measurement of Cl derived ^{38}Ar ($^{38}Ar_{Cl}$). This is important for the study of excess argon because Cl may be associated with excess argon in melt inclusions [*Esser et al.*, 1997]. Irradiation information and analytical details are given in Table 1.

[16] The $^{40}Ar/^{39}Ar$ analyses were completed at the New Mexico Geochronology Research Laboratory. Most $^{40}Ar/^{39}Ar$ ages were determined by single-crystal laser fusion of sanidine. One advantage of this technique is the ability to identify and eliminate anomalously aged crystals from age calculations [*Deino and Potts*, 1990, 1992]. Crystals that had apparent ages significantly older than the main population were considered to be xenocrysts. In addition, crystals with K/Ca values or radiogenic yields significantly outside the main population were not used in age calculations. In rare cases, anomalously young crystals were eliminated from age calculations and considered to represent altered crystals that have undergone Ar loss. Fish Canyon tuff (FCT) sanidine was used as a neutron flux monitor with an assigned age of 28.02 Ma [*Renne et al.*, 1998]. FCT sanidine is widely used due to its homogeneous nature, although its assigned age is debated [*Lanphere and Baadsgaard*, 2001]. All referenced ages reported herein were recalculated based on this monitor age for comparison with ages in this study. J factors were determined by single-crystal laser fusion of irradiated sanidine crystals. Ages were calculated using decay constants following *Steiger and Jäger* [1977]. For single-crystal sanidine analyses, calculated mean age is weighted mean age and the error is the weighted error of the mean [*Taylor*, 1982], multiplied by the square root of the mean square weighted deviation (MSWD), when MSWD>1, and include uncertainties in interfering reactions and J factors. Uncertainties are reported at $\pm 2\sigma$, unless otherwise noted.

4. Results

4.1. Upper Bandelier Tuff

[17] Sanidine from four samples of UBT were dated, including unaltered outflow facies ignimbrite (EP-44), the Plinian fall deposit (EP-43), and two samples of intracaldera UBT (EP-1, EP-28; Table 2). Ignimbrite sample EP-44 from east of the caldera (Figure 1) gave an age of 1.256 ± 0.010 Ma (Figure 2). The sample has a well-defined population of apparent ages and a $^{40}Ar/^{36}Ar$ isochron intercept of 297.1 ± 3.8, indistinguishable from the atmospheric value of 295.5. Radiogenic yields range from 21.1% to 97.3% and the sample contains no anomalously aged crystals. The fall deposit beneath the ignimbrite gives an age of 1.232 ± 0.017 Ma after excluding numerous anomalously old crystals, which could have been xenocrysts inherited during a vent-widening event in the earliest stages of the UBT eruption. Intracaldera UBT contains more anomalously old crystals than the outflow facies ignimbrite and one sample (EP-28) yields an imprecise age due to the wide range in ages of sanidine crystals (Table 2). Xenocrysts in intracaldera UBT could have also resulted from a vent-widening event during the latter part of the UBT eruption, when the eruption column was lower and the tuff underwent shorter transport distances. The age of 1.256 ± 0.010 Ma for EP-44 is considered the "preferred age" for the UBT in Table 2 because this sample had no anomalously aged crystals and gave more precise $^{40}Ar/^{39}Ar$ analysis than the other three samples from this unit. Considering 2σ uncertainties, this age is statistically indistinguishable from published ages (recalculated using 28.02 Ma FCT sanidine flux monitor age) for the UBT of *Izett and Obradovich* [1994] (1.244 ± 0.018 Ma) and *Spell et al.* [1996] (1.230 ± 0.016 Ma).

Table 2. Summary of ^{40}Ar/^{39}Ar Ages for the First Valles caldera Ring Fracture Rhyolite, Postcollapse Intracaldera Units, and Upper Bandelier Tuff[a]

Map	Sample	Unit	Rock Type	n[b]	MSWD[c]	Age ± 2σ, [d,e] Ma	Final Age Determination ± 2σ, Ma
			Ring Fracture Rhyolite				
1	EP-42	Cerro del Medio (Valle Grande Member)	rhyolite lava	28	0.31	1.210 ± 0.023	pooled age 1.229 ± 0.017[f]
2	EP-39	Cerro del Medio (Valle Grande Member)	rhyolite lava	34	1.95	1.239 ± 0.028	
			Resurgent Dome Rhyolites				
3	EP-7	Redondo Creek Member	pumiceous rhyolite lava	20	0.95	1.208 ± 0.017	age range 1.208 ± 0.017 to 1.239 ± 0.017[g]
4	F03-52	Redondo Creek Member	rhyolite lava	14	0.14	1.227 ± 0.020	
5	F03-53	Redondo Creek Member	rhyolite lava	12	0.22	1.235 ± 0.028	
6	EP-10HF	Redondo Creek Member	rhyolite lava	23	0.91	1.239 ± 0.017	
7	EP-14	Deer Canyon Member	lithic tuff	12	1.42	1.229 ± 0.013	age range 1.229 ± 0.013 to 1.283 ± 0.017[g]
8	EP-15	Deer Canyon Member	lithic tuff	9	0.46	1.245 ± 0.027	
9	F03-14b	Deer Canyon Member	rhyolite lava	13	0.14	1.254 ± 0.025	
10	EP-31	Deer Canyon Member	lithic tuff	14	0.70	1.257 ± 0.022	
11	EP-34	Deer Canyon Member	rhyolite lava	11	0.87	1.262 ± 0.023	
12	EP-2	Deer Canyon Member	lithic tuff	25	1.27	1.274 ± 0.022	
13	EP-29	Deer Canyon Member	lithic tuff	14	2.23	1.274 ± 0.022	
14	EP-32	Deer Canyon Member	rhyolite lava	31	1.69	1.283 ± 0.017	
			Upper Bandelier Tuff				
15	EP-43	upper Bandelier Tuff	Plinian fall deposit	8	1.82	1.232 ± 0.017	preferred age 1.256 ± 0.010 (EP-44)[h]
16	EP-44	outflow facies upper Bandelier Tuff	ignimbrite	33	1.07	1.256 ± 0.010	
17	EP-1	intracaldera upper Bandelier Tuff	welded ignimbrite	18	3.37	1.262 ± 0.016	
18	EP-28	intracaldera upper Bandelier Tuff	welded ignimbrite	24	3.56	1.300 ± 0.031	

[a]*Phillips et al.* [2007] provide complete data and are available at http://geoinfo.nmt.edu/publications/openfile/argon/home.html.
[b]Number of analyses used to calculate weighted mean age.
[c]Mean square of weighted deviates; a goodness of fit parameter.
[d]Weighted mean ages and plateau ages calculated by weighting each analysis by the inverse of the variance and errors calculated based on the work by *Taylor* [1982].
[e]All ages are weighted mean ages, calculated from single-crystal laser fusion analysis of sanidine.
[f]Pooled ages; a weighted mean age is calculated for all crystals from multiple samples from the same geologic unit, by the same methods used to calculate individual weighted mean ages. Used if ages from multiple samples are statistically indistinguishable.
[g]Age ranges; a range of ages for a geologic unit. Used if a geologic unit is physically variable and occurs in multiple isolated localities, or if field evidence shows the unit was erupted over a span of time.
[h]Preferred age; the age of a single sample that is found to be the most precise amongst multiple samples from a geologic unit. Used if the ^{40}Ar/^{39}Ar age of one sample is clearly more precise than ages for other samples within the unit.

4.2. Deer Canyon Member

[18] The Deer Canyon Member includes rhyolitic lavas, lithic tuffs, and breccias and its intraunit lithology and stratigraphy are variable in different portions of the caldera. Sanidine phenocrysts from three Deer Canyon lavas (F03-14b, EP-34, EP-32) yield ages of 1.254 ± 0.025 Ma, 1.262 ± 0.023 Ma and 1.283 ± 0.017 Ma (Table 2). These three ages are indistinguishable at the 2σ confidence level. Radiogenic yields are above 76% for EP-32 and EP-34 and range from 14.5% to 93.3% for F03-14b.

[19] Five Deer Canyon tuff samples (EP-31, EP-2, EP-29, EP-14, EP-15) range in age from 1.229 ± 0.013 Ma to 1.274 ± 0.022 Ma (Table 2). K/Ca values of the sanidine in EP-31 and EP-14 are consistent within each sample, whereas K/Ca values in EP-2, EP-29, and EP-15 are more variable. Radiogenic yields are >60% for all crystals except in EP-31, for which radiogenic yields range from 25.3% to 93.6%. Samples EP-2 and EP-15 contain numerous anomalously old crystals, interpreted as xenocrysts, whereas EP-29, EP-14, and EP-31 exhibit fewer anomalously old crystals. Inverse isochron plots show that EP-2 contains a trapped argon component with a ^{40}Ar/^{36}Ar intercept of 400 ± 80, greater than the atmospheric value of 295.5. The other samples have ^{40}Ar/^{36}Ar isochron intercepts indistinguishable from atmosphere.

[20] The eight Deer Canyon Member lavas and tuffs range in age from 1.229 ± 0.013 Ma to 1.283 ± 0.017 Ma (Figure 2). The ages do not all overlap at the 2σ confidence level, so an age range is reported for this unit (Table 2). In addition, the physical and spatial variability of the Deer Canyon Member demonstrate that all eruptive events did not necessarily occur contemporaneously.

Figure 2. The ^{40}Ar/^{39}Ar age probability distribution diagrams. The age for Cerro del Medio is a pooled age for two samples from the same lobe. The upper Bandelier Tuff age is from the outflow facies ignimbrite and is the preferred age for this unit. Open circles denote analyses excluded from weighted mean age, and open probability curve represents the curve that results if these analyses are included. Older xenocrysts are present in some samples [see *Phillips et al.*, 2007].

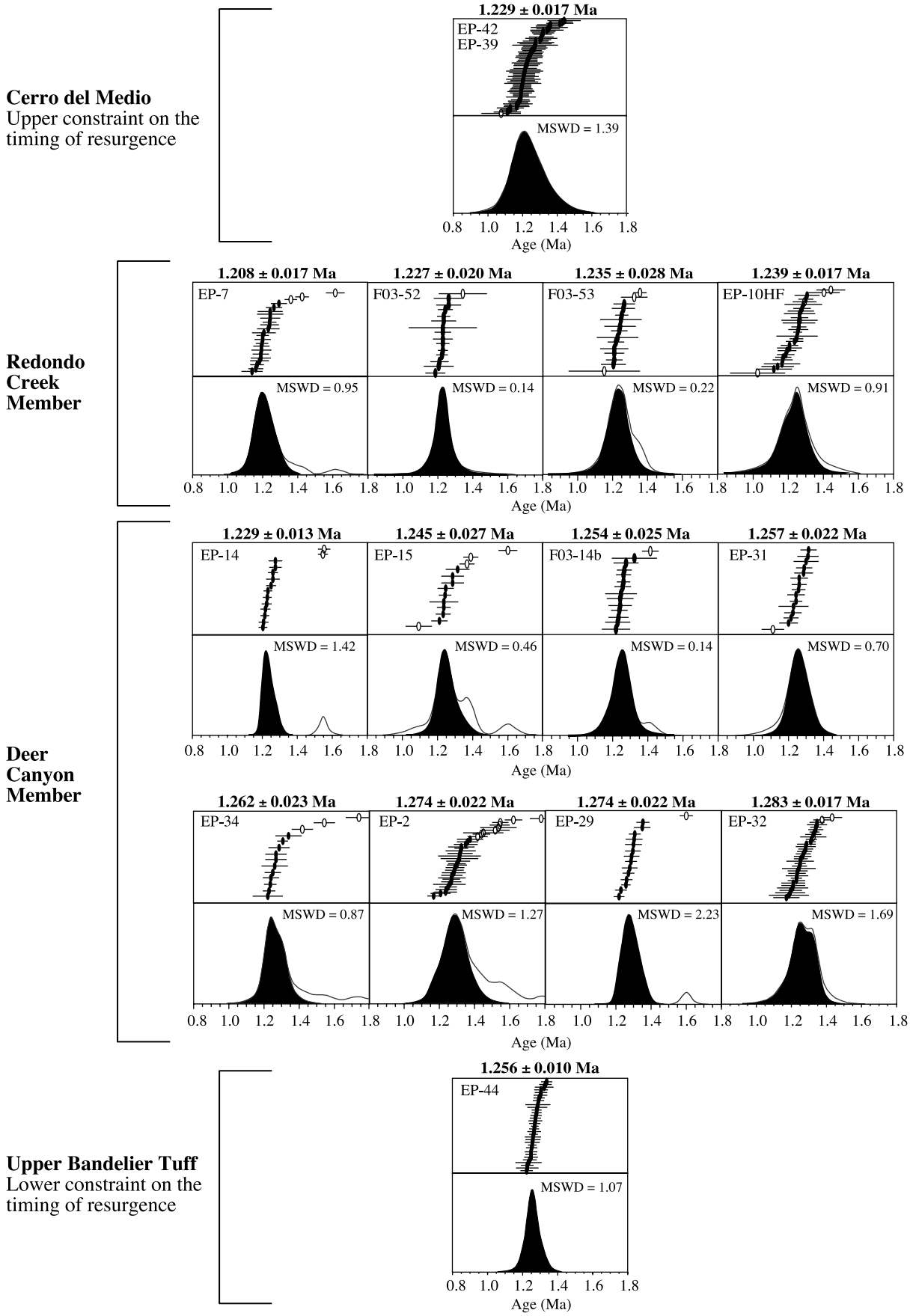
Cerro del Medio
Upper constraint on the timing of resurgence
1.229 ± 0.017 Ma
EP-42
EP-39
MSWD = 1.39
Redondo Creek Member
1.208 ± 0.017 Ma
EP-7
MSWD = 0.95
1.227 ± 0.020 Ma
F03-52
MSWD = 0.14
1.235 ± 0.028 Ma
F03-53
MSWD = 0.22
1.239 ± 0.017 Ma
EP-10HF
MSWD = 0.91
Deer Canyon Member
1.229 ± 0.013 Ma
EP-14
MSWD = 1.42
1.245 ± 0.027 Ma
EP-15
MSWD = 0.46
1.254 ± 0.025 Ma
F03-14b
MSWD = 0.14
1.257 ± 0.022 Ma
EP-31
MSWD = 0.70
1.262 ± 0.023 Ma
EP-34
MSWD = 0.87
1.274 ± 0.022 Ma
EP-2
MSWD = 1.27
1.274 ± 0.022 Ma
EP-29
MSWD = 2.23
1.283 ± 0.017 Ma
EP-32
MSWD = 1.69
Upper Bandelier Tuff
Lower constraint on the timing of resurgence
1.256 ± 0.010 Ma
EP-44
MSWD = 1.07
0.8 1.0 1.2 1.4 1.6 1.8
Age (Ma)

Figure 2

[21] The lack of published age determinations for the Deer Canyon Member has been attributed to difficulties in finding unaltered outcrops [*Spell and Harrison*, 1993]. Even though the unit does show significant alteration [*Chipera et al.*, 2007], we have found unaltered sanidine phenocrysts that provide meaningful ^{40}Ar/^{39}Ar ages. *Doell et al.* [1968] obtained a K/Ar age on sanidine from the Deer Canyon Member of 1.25 ± 0.11 Ma. This age is similar to those obtained in this study, but is inconsistent with ages of other eruptive units reported by *Doell et al.* [1968].

4.3. Redondo Creek Member

[22] Sanidine from four Redondo Creek Member rhyolite lavas (EP-7, F03-52, F03-53, EP-10HF) were dated (Table 2). Plagioclase is a common phenocryst phase in the Redondo Creek Member and analyses of plagioclase crystals were eliminated from ^{40}Ar/^{39}Ar data. Once these analyses are deleted, K/Ca values range from 14.8 to 47.0. Anomalously old crystals were eliminated from age calculations in all four samples and interpreted as xenocrysts. Redondo Creek Member samples yield near-Gaussian populations with weighted mean ages of 1.208 ± 0.017 Ma, 1.227 ± 0.020 Ma, 1.235 ± 0.028 Ma, and 1.239 ± 0.017 Ma (Figure 2). An age range is reported for this unit because it is found interspersed throughout the west central resurgent dome and is physically variable, consisting of rhyolitic domes, dikes, flows, and interlayered tuffs [*Smith et al.*, 1970], implying that it did not erupt during a single post-collapse event. Two Redondo Creek samples are excluded from this discussion because of multiple crystal populations and/or alteration [*Phillips*, 2004].

[23] Existing geochronological data from the Redondo Creek Member are limited. *Doell et al.* [1968] reported a K/Ar age of sanidine of 1.28 ± 0.06 Ma, which is significantly older than the ages for the UBT obtained in their study. A fission track age of 1.7 ± 0.12 Ma (1σ) was reported by *Marvin and Dobson* [1979], an age which is clearly unreasonable given the agreement among more recently reported ages for the UBT. *Goff and Gardner* [2004] reported a K-Ar age of 1.23 ± 0.02 Ma on a sample from the type locality at the head of Redondo Creek.

4.4. Cerro del Medio

[24] Feldspar crystals from two samples (EP-42, EP-39) from one of the oldest flow lobes of Cerro del Medio were dated (Table 2). The K/Ca values in feldspar phenocrysts range from 13.3 to 40.6. Radiogenic yields are variable, ranging from 29.2% to 100%; however most are above 80%. After excluding two anomalously young crystals and two anomalously old crystals, sample EP-42 gives a weighted mean age of 1.210 ± 0.023 Ma. Sample EP-39 yields a weighted mean age of 1.239 ± 0.028 Ma. The pooled age (weighted mean age for all crystals) for the two samples is 1.229 ± 0.017 Ma (Figure 2 and Table 2). The pooled age is used because the two ages are indistinguishable at the 2σ confidence interval and the samples are of the same lithology and eruptive history. The precision is increased by pooling the ages because of the large number of crystals (62) analyzed from these samples. This age is considered the best estimate of the time since one of the earliest Cerro del Medio eruptions.

[25] A sample from another early flow lobe of Cerro del Medio gave an age of 1.316 ± 0.059 Ma, but the low K_2O content of feldspars analyzed from this sample results in large uncertainties on each analysis and therefore a relatively large error on the weighted mean age, yielding what is considered an unreliable age for Cerro del Medio [*Phillips*, 2004].

[26] Published ^{40}Ar/^{39}Ar ages for Cerro del Medio exhibit some disagreement. Many factors contribute to a final reported age and comparisons between laboratories often yield systematic differences, especially for relatively young rocks such as those dated here. *Spell and Harrison* [1993] reported a pooled isochron age of 1.138 ± 0.022 Ma for samples from both an older and a younger flow lobe [*Gardner et al.*, 2006]. In addition to their different sampling approach, a potential cause for the significantly younger age is the unusually high $(^{40}Ar/^{39}Ar)_K$ correction factor of 0.0418 reported for the University of Michigan Ford Reactor by *Spell and Harrison* [1993]. *Singer and Brown* [2002] also call attention to analytical and methodological problems with *Spell and Harrison* [1993] and suggest the possibility that the HCl cleaning procedure used to remove glass from sanidine crystals was inadequate, and resulted in ^{40}Ar/^{36}Ar intercepts less than the atmospheric value of 295.5. Overall, the data collected here benefit from improved operating conditions that include the use of a shielded irradiation facility, lower mass 36 backgrounds, additional neutron flux monitoring, and a CO_2 laser that allows complete extraction of the argon from the sample. On the basis of these improvements, we suggest that our age determination for Cerro del Medio is more accurate than the data reported by *Spell and Harrison* [1993].

[27] *Izett and Obradovich* [1994] do not report ages for the flow lobe dated in this study. However, their oldest Cerro del Medio age of 1.228 ± 0.017 Ma is nearly identical to our age of 1.229 ± 0.017 Ma.

4.5. Excess Argon

[28] Excess argon ($^{40}Ar_E$) is the component of ^{40}Ar incorporated by processes other than the in situ radioactive decay of ^{40}K [*Dalrymple and Lanphere*, 1969]. We carried out two experiments to investigate the effects of $^{40}Ar_E$ in the UBT and the Deer Canyon Member because of the similarity in ages of the units dated and because *Winick et al.* [2001] identified $^{40}Ar_E$ in the UBT. In addition, $^{40}Ar_E$ was identified in the Cerro Santa Rosa I dome, a Valles caldera postcollapse ring fracture dome with an ^{40}Ar/^{39}Ar age of 936 ± 8 ka [*Singer and Brown*, 2002].

4.5.1. Melt Inclusion-Bearing Quartz

[29] Melt inclusion-bearing quartz crystals from UBT sample EP-44 and Deer Canyon tuff sample EP-31 were measured to assess the amount of ^{40}Ar that resides in melt inclusions and calculate the effect that $^{40}Ar_E$ would have on the apparent ^{40}Ar/^{39}Ar age of sanidine phenocrysts, using methods similar to those employed by *Winick et al.* [2001]. Because quartz contains no K, ^{40}Ar/^{39}Ar analysis of melt inclusion-bearing quartz measures ^{40}Ar in melt inclusions only. Melt inclusion-bearing quartz was separated by standard magnetic, heavy liquid, and hand picking techniques. Separates (241 mg EP-44; 235 mg EP-31) were step heated in a Mo double-vacuum resistance furnace in nine heating steps.

Table 3. Summary of ^{40}Ar/^{39}Ar Results From Melt Inclusion-Bearing Quartz Experiment

Sample	Unit	Integrated Age, Ma
EP-44	outflow facies upper Bandelier Tuff	5.66 ± 0.43
EP-31	Deer Canyon Member tuff	35.2 ± 2.4

[30] UBT melt inclusion-bearing quartz gives an integrated age of 5.66 ± 0.43 Ma (Table 3). Most (79%) of the ^{39}Ar gas was released in the first (A) heating step, for which an age of 4.13 ± 0.20 Ma was obtained. Melt inclusion-bearing quartz from Deer Canyon tuff yields an integrated age of 35.2 ± 2.4 Ma (Table 3). Similarly, 62% of the ^{39}Ar gas was released during the first heating step, which gives an age of 21.48 ± 1.58 Ma. Cl/K ratios do not vary significantly between the different heating steps for either sample [*Phillips et al.*, 2007].

4.5.2. Etched Sanidine

[31] Single-crystal laser fusion of sanidine from UBT sample EP-44 and Deer Canyon tuff sample EP-31 showed that they contain no anomalously old crystals. Sanidine crystals were crushed and etched in dilute hydrofluoric acid (HF) to remove melt inclusions, which are possible hosts for ^{40}Ar$_E$ [*Esser et al.*, 1997]. Sanidine separates were crushed to approximately 90–125 μm and a split was subsequently removed. This is termed the "surface etched" split because

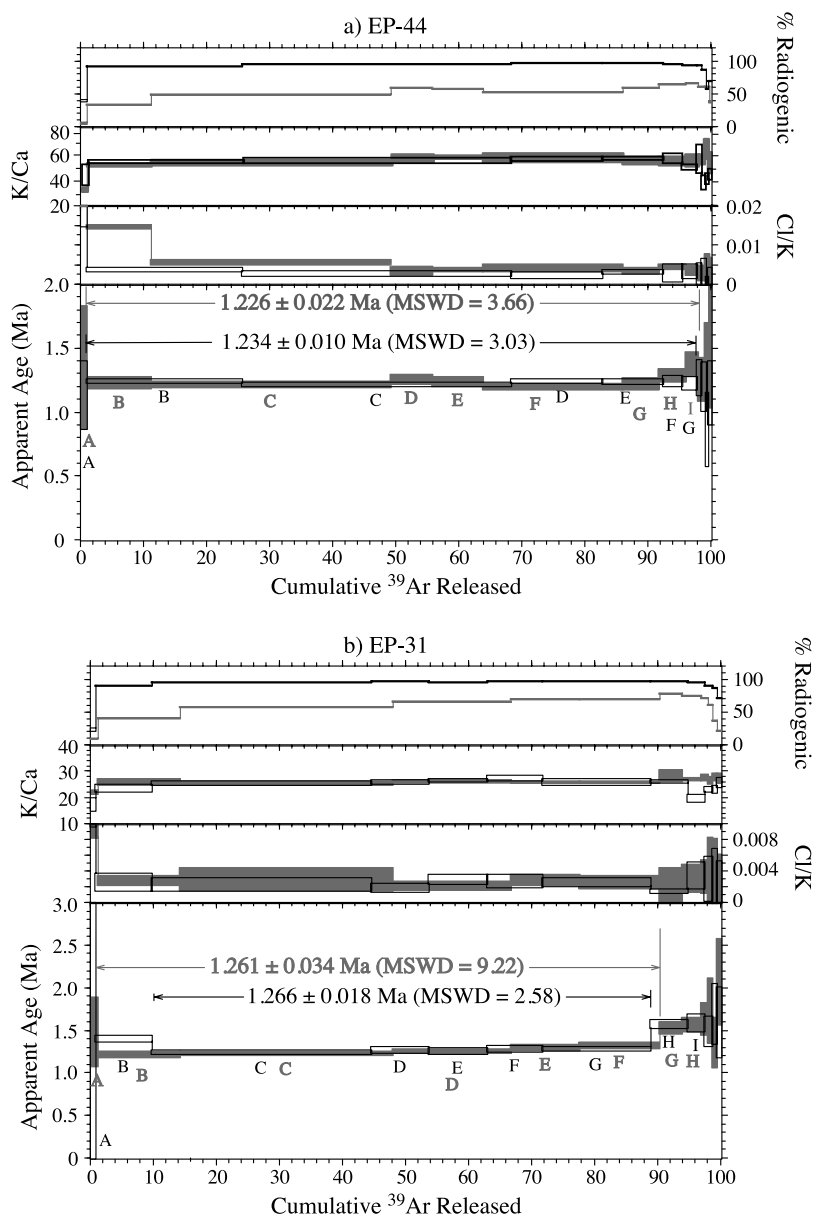

Figure 3. Age spectra for crushed and etched sanidine used in the excess argon study for (a) UBT sample EP-44 and (b) Deer Canyon tuff sample EP-31. Black open spectra are for "crushed and etched" portion and gray spectra are for "surface etched" portion. Labels for high-temperature steps were removed for clarity. Each sample was heated in 11 or 12 incremental heating steps.

Table 4. Summary of ^{40}Ar/^{39}Ar Results From Etched Sanidine Experiment

Sample	Unit	Treatment	^{40}Ar* in Steps Used to Calculate Plateau Age, %	n[a]	MSWD	Plateau Age, Ma
EP-44	outflow facies upper Bandelier Tuff	surface etched	33.6–66.2	8	3.66	1.226 ± 0.022
EP-44	outflow facies upper Bandelier Tuff	crushed and etched	92.4–96.9	6	3.03	1.234 ± 0.010
EP-31	Deer Canyon Member tuff	surface etched	41.0–69.6	5	9.22	1.261 ± 0.034
EP-31	Deer Canyon Member tuff	crushed and etched	95.3–97.3	5	2.58	1.266 ± 0.018

[a]The number of steps used to calculate plateau age.

only the surfaces of the sanidine crystals were subjected to HF etching (prior to crushing). The remaining crushed sample was then etched in 15% HF acid for 15–20 min. This is termed the "crushed and etched" split because the crushed sample was subjected to HF etching. This sample preparation procedure was designed to remove trapped melt inclusions in the "crushed and etched" split and evaluate the effect on the ^{40}Ar/^{39}Ar apparent age by comparison to the "surface etched" split. Both splits from each sample were step heated with a CO_2 laser.

[32] In EP-44 (UBT), the radiogenic yield in the "crushed and etched" portion is considerably higher than in the "surface etched" portion (Figure 3a and Table 4). There is not a well-defined correlation between Cl/K and apparent age for either of the splits. The "crushed and etched" portion yields a plateau age of 1.234 ± 0.010 Ma and the "surface etched" portion yields a plateau age of 1.226 ± 0.022 Ma, ages that overlap at the 2σ confidence level (Table 4). The "surface etched" plateau age is not significantly different from the single-crystal laser fusion age for EP-44 of 1.256 ± 0.010 Ma.

[33] Similarly, for sample EP-31 (Deer Canyon tuff), radiogenic yields for the "crushed and etched" portion are higher than those for the "surface etched" portion (Figure 3b and Table 4). Cl/K does not exhibit a marked relationship to apparent age. This sample yields plateau ages of 1.266 ± 0.018 Ma for the "crushed and etched" portion and 1.261 ± 0.034 Ma for the "surface etched" portion (Table 4). These ages are indistinguishable at 2σ confidence level and are also statistically the same as the single-crystal age for this sample of 1.257 ± 0.022 Ma.

5. Discussion

5.1. Implications of ^{40}Ar/^{39}Ar Ages for the Duration of Resurgence

[34] Structural and stratigraphic relationships show that caldera collapse and concurrent eruption of the UBT occurred prior to resurgence. Therefore the age of the UBT (1.256 ± 0.010 Ma) is the lower constraint on the timing of resurgence. One of the oldest flow lobes of Cerro del Medio (1.229 ± 0.017 Ma) is the upper time constraint and the duration of resurgence is the difference in ages between the UBT and this lobe of Cerro del Medio (Figures 4 and 5). Our study is especially conducive to determining the relative age difference between these two eruptive units because both samples were dated in the same laboratory, using consistent procedures and similar laboratory conditions.

[35] Without considering uncertainties, the difference between the weighted mean ages of the UBT and Cerro del Medio is 27 ka. Uncertainties are quoted at the 2σ confidence level, which signifies that there is a 95% chance that the actual value is within the error limits. Taking into account the uncertainties on the ages of the two units, the minimum age difference is exactly zero. The maximum age difference is 54 ka. Therefore the time window between the two eruptions is 27 ± 27 ka (2σ), which is the best estimate

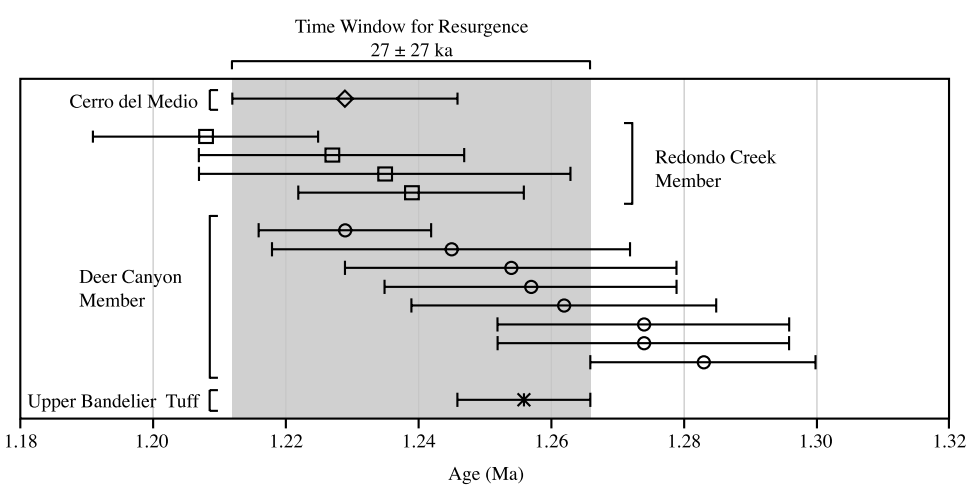

Figure 4. Comparison of ages of the upper Bandelier Tuff and postcollapse units, with associated uncertainties (2σ). The time window for resurgence (27 ± 27 ka) is shaded in gray and constrained by the ages and uncertainties of Cerro del Medio and the upper Bandelier Tuff. The maximum time window for resurgence is 54 ka (2σ).

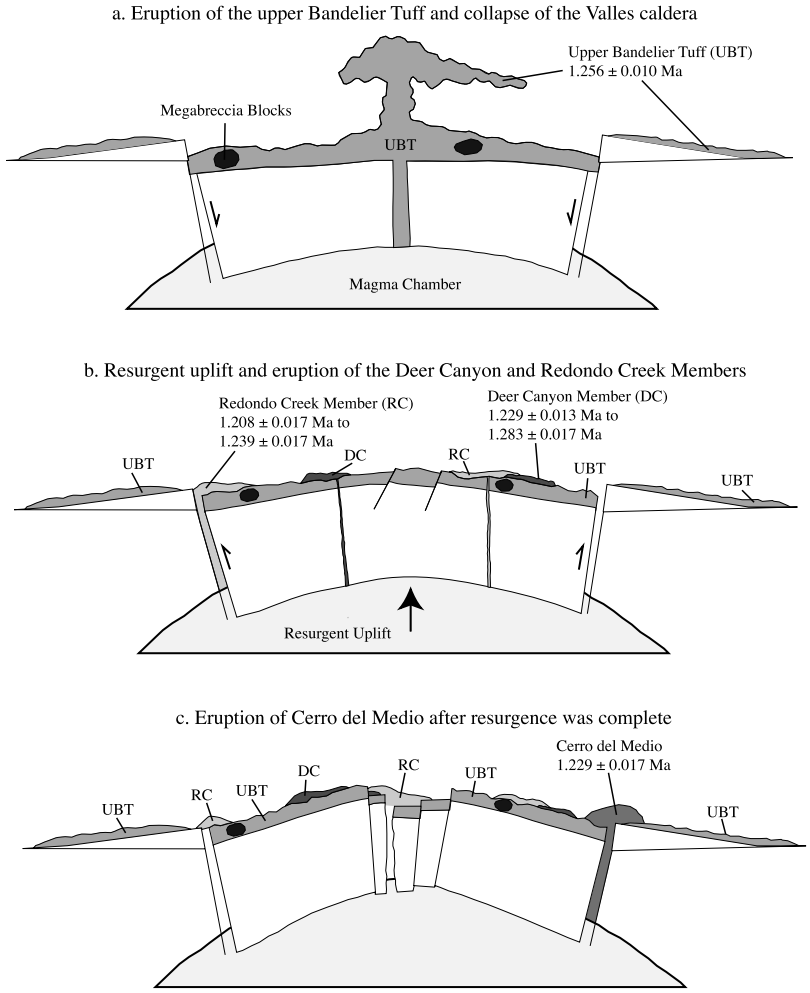

Figure 5. Model of the history of the Valles caldera during caldera collapse, resurgence, and earliest ring fracture volcanism (partially after *Smith and Bailey* [1968]). Unit thicknesses and horizontal and vertical distances are not to scale. Caldera fill, which consists of debris flow deposits and lacustrine and fluvial sediments deposited during collapse and resurgence, is not depicted. (a) Eruption of the upper Bandelier Tuff from a central vent and concurrent collapse of the Valles caldera resulting in thick accumulations of both intracaldera and extracaldera upper Bandelier Tuff [*Self et al.*, 1986]. Megabreccia blocks slid into the caldera due to catastrophic failure of the caldera walls. (b) Resurgent uplift and eruption of the Deer Canyon and Redondo Creek members. It is possible that minor eruptions of these units took place before resurgence commenced. Faults developed on the resurgent dome, which were utilized as conduits for intracaldera magmas. (c) Eruption of earliest ring fracture dome, Cerro del Medio after resurgent uplift ceased.

for the duration of resurgence in the Valles caldera (Figure 4). On the basis of these uncertainties, there is a 95% probability that resurgence was complete within 54 ka. These data also confirm that resurgence commenced relatively soon after caldera collapse and highlights the physicomagmatic differences between resurgence at the Valles caldera and resurgence at Yellowstone and Long Valley, calderas that last erupted at 0.6 Ma and 0.7 Ma, respectively, and have experienced recent uplift [*Pelton and Smith*, 1979; *Savage and Clark*, 1982].

[36] Redondo Peak, the summit of the resurgent dome, is ~840 m above Valle Grande, which is part of the undomed caldera floor. However, the actual maximum height to which the resurgent dome rose is probably much greater because the caldera floor in Valle Grande is concealed by a considerable thickness of alluvium and caldera fill material. In addition, erosion of the resurgent dome has further obscured the maximum height of resurgent uplift, and we cannot account for how much the resurgent dome may have deflated. Taking these factors into consideration, the relief of the resurgent dome from the surrounding caldera floor is estimated to be at least 1000 m. Therefore using the maximum period for resurgence of 54 ka, a minimum resurgence rate of 1.9 cm/yr is calculated. Using 27 ka for the duration of resurgence gives a resurgence rate of 3.7 cm/yr. The uncertainties on ^{40}Ar/^{39}Ar ages and the unknown nature of resurgence as a continuous or intermittent process permit us to report only an average resurgence rate, which is at least 1.9 cm/yr and possibly as high as 100 cm/yr if resurgence was complete within a millennium.

[37] Despite uncertainties associated with the resurgence rate at the Valles caldera, our reported range is similar to rates reported for other large ignimbrite-producing calderas. Raised wave-cut terraces at Iwo-Jima caldera in the Izu-Bonin volcanic arc, located about 1150 km south of Tokyo in the Pacific Ocean, indicate uplift rates averaging 15–20 cm/yr during the last 500–700 years [*Kaizuka et al.*, 1989; *Fisher et al.*, 1997]. A comparable rate of 15.6 cm/yr from 1002 to 1992 A.D. was reported for the Yenkahe Resurgent Block, Tanna, Vanuatu using emerged reef terraces [*Chen et al.*, 1995]. The Campi Flegrei caldera, located near Naples, Italy, is a complex resurgent caldera that has undergone two recent episodes of major uplift (1969–1972 and 1982–1984). During these episodes, average uplift rates of approximately 1.4 mm/day (51 cm/yr) were recorded [*Orsi et al.*, 1999]. The intermittent nature of resurgence in this caldera is exhibited by subsidence that occurred after both uplift episodes.

[38] At Yellowstone caldera, resurgence rates as high as 2.7 cm/yr have been reported based on precise leveling measurements [*Pelton and Smith*, 1979; *Jackson et al.*, 1984], but uplift is spatially and temporally variable, and subsidence has also been recorded in recent years [*Smith and Braile*, 1994; *Dzurisin et al.*, 1999]. Maximum resurgence rates reported for Long Valley caldera are as high as 5 cm/yr [*Savage and Clark*, 1982] and the most recent seismic unrest (1978–1999) resulted in uplift of 80 cm, at an average rate of 3.8 cm/yr [*Sorey et al.*, 2003]. As stated previously, recent uplift at Yellowstone and Long Valley may represent different processes than those that caused resurgent uplift of the Valles caldera. Uplift at Yellowstone and Long Valley is occurring 600 to 700 ka after the last major eruptions at these calderas, whereas resurgent uplift of the Valles caldera was complete within 54 ka of caldera collapse and the concurrent eruption of the UBT.

5.2. Postcollapse Intracaldera Units

[39] The Deer Canyon and Redondo Creek members stratigraphically overlie the UBT, confirming that they were erupted after caldera collapse (Figure 5). Seven of the eight samples from the Deer Canyon Member yield ages that are statistically indistinguishable from the age of the UBT (1.256 ± 0.010 Ma; Figure 2). Sample EP-14 has an age of 1.229 ± 0.013 Ma, indicating that, based on 2σ uncertainties, it is at least 4 ka younger than the UBT (Figure 4). The field relationships and ages of samples from the Deer Canyon Member suggest that it likely began to erupt immediately after the UBT, and continued erupting during resurgence.

[40] The ^{40}Ar/^{39}Ar ages for four samples from the Redondo Creek Member range from 1.208 ± 0.017 Ma to 1.239 ± 0.017 Ma (Figure 2), which are indistinguishable at the 2σ confidence interval. The ages for three of the samples are statistically indistinguishable from the age of the UBT (1.256 ± 0.010 Ma). The age of 1.208 ± 0.017 Ma for EP-7 is significantly younger than the UBT (Figure 4) and implies that some Redondo Creek rhyolites were erupted at least 21 ka after eruption of the UBT and caldera collapse.

[41] The Redondo Creek Member is found overlying the UBT and/or the Deer Canyon Member. Although local field relationships show that the Deer Canyon Member in some areas predates the Redondo Creek Member [*Smith et al.*, 1970], the ^{40}Ar/^{39}Ar age ranges for the two units overlap (Figure 4). The ages obtained in this study do not preclude the possibility that the Redondo Creek Member was erupted immediately after the UBT, but also show that some eruptions of the Redondo Creek Member occurred during resurgence. Field relationships also suggest that the Redondo Creek Member was erupted prior to and during resurgence based on the following observations: (1) it is interlayered with caldera fill sediments, (2) it is faulted and deformed from resurgent uplift, and (3) some Redondo Creek rhyolites were erupted along fractures and faults that developed during resurgence [*Doell et al.*, 1968; *Bailey et al.*, 1969; *Smith et al.*, 1970]. The complex nature of the field relationships and the range in ages for the Redondo Creek Member do not permit a decisive conclusion regarding the time at which resurgence commenced. Resurgence could have begun immediately after collapse, or there may have been a short time interval between collapse and resurgence.

5.3. Xenocrysts in Postcollapse Units

[42] Because of the similarity in ages of the volcanic rocks discussed herein, a thorough evaluation of xenocrysts in postcollapse units is merited. It is important to note that the number of xenocrysts identified by ^{40}Ar/^{39}Ar analyses is not necessarily representative of the actual number of xenocrysts in a sample. If the appearance of xenocrysts distinguished them from phenocrysts in a sample, then they were excluded from ^{40}Ar/^{39}Ar mineral separates during sample preparation. However, in some samples, xenocrysts and phenocrysts might not be distinct and therefore impossible to cull by mineral separation techniques. As previously stated, crystals with ages significantly older than the main population are considered to be xenocrysts and eliminated from ^{40}Ar/^{39}Ar single-crystal age calculations. However, the presence of xenocrysts with ages indistinguishable from the age of the rock is possible. The following section addresses the concern of similar aged xenocrysts in postcollapse units, particularly the presence of UBT xenocrysts in the Deer Canyon and Redondo Creek members, and Cerro del Medio, and focuses on the compositional differences between feldspars from these units.

[43] The abundance and ages of xenocrysts vary significantly from sample to sample in the Deer Canyon and Redondo Creek members. Many crystals give ages similar to the LBT, suggesting that they are xenocrysts from that unit (Figure 2). The crystals yielding ages intermediate between the age of the LBT and the main population of crystals are probably either partially reset LBT xenocrysts or crystals from the Cerro Toledo rhyolites. The abundance of xenocrysts in one Deer Canyon tuff sample (EP-2) could be due to an explosive eruption and vent-widening event, a phenomenon that has been documented at other calderas [e.g., *Hu et al.*, 1994; *Chen et al.*, 1996; *Gansecki et al.*, 1996; *Spell et al.*, 2001]. There is no simple apparent relationship between the number and distribution of xenocrysts in Deer Canyon or Redondo Creek samples and their location in the caldera.

[44] Despite the similar ages for the Deer Canyon Member, the Redondo Creek Member, and the UBT, there are significant differences in the K/Na ratio of feldspars (Figure 6), the Ba concentration in feldspars, and the

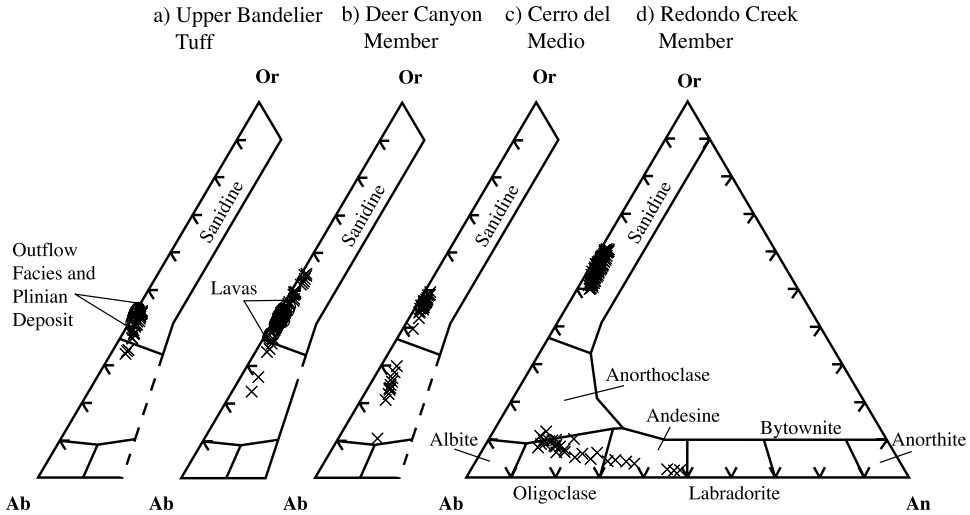

Figure 6. Feldspar ternary plots (orthoclase (Or), albite (Ab), anorthite (An)). (a) Upper Bandelier Tuff (open circles indicate outflow facies ignimbrite and Plinian fall deposit; crosses indicate intracaldera welded tuffs). (b) Deer Canyon Member (open circles indicate lavas; crosses indicate tuffs). (c) Cerro del Medio rhyolite lavas from southern flow lobe. (d) Redondo Creek Member rhyolite lavas. Electron microprobe analytical conditions used: 15 kV, 20 nA, 10 μm beam size. See *Phillips et al.* [2007] for complete data and analytical details.

composition of melt inclusions between the units [*Phillips et al.*, 2007]. These observations imply that at least some of the feldspar crystals within the Deer Canyon and Redondo Creek members are indeed phenocrysts. Feldspar crystals from the Deer Canyon Member range from $Or_{34}Ab_{63}An_3$ to $Or_{51}Ab_{47}An_1$ whereas UBT feldspars analyzed in this study exhibit a smaller range from $Or_{34}Ab_{63}An_3$ to $Or_{44}Ab_{55}An_1$ (Figure 6). *Caress* [1996] identified feldspars from the UBT ranging from Or_{25} to Or_{44}. Redondo Creek Member feldspars exhibit little overlap with feldspar compositions from the UBT. They include numerous anorthoclase, oligoclase, and andesine analyses in addition to sanidine compositions ranging from $Or_{51}An_{46}Ab_3$ to $Or_{59}An_{39}Ab_2$ (Figure 6). In addition, Deer Canyon Member feldspars range in BaO concentration from below detection limit to 0.48 wt % with an average of 0.04 wt % (n = 103), whereas the Redondo Creek Member includes feldspars with Ba concentrations as high as 1.59 wt % with an average of 0.68 wt % (n = 98). Upper Bandelier Tuff feldspars exhibit a smaller range in BaO concentration, from below detection limit to 0.12 wt % with an average of 0.03 wt % (n = 46). Electron microprobe analyses of glass show that two melt inclusions in the Deer Canyon Member and five melt inclusions in the Redondo Creek Member are distinct from glass compositions of the UBT, also indicating that it is not likely that all sanidine crystals in these units are xenocrysts inherited from the UBT [*Phillips et al.*, 2007].

[45] Xenocrystic contamination appears to be less common in Cerro del Medio rhyolites than in most Deer Canyon and Redondo Creek samples. Two xenocrysts significantly outside the main age population of crystals were found in the two Cerro del Medio samples. If ubiquitous UBT xenocrysts were present in Cerro del Medio, the age determination for this unit could be compromised, as well as the calculations of resurgence rate and duration. However, at least some phenocrystic sanidine in Cerro del Medio is indicated by ^{40}Ar/^{39}Ar single-crystal analysis and electron microprobe analysis of feldspar chemistry (Figure 6). The combined MSWD for the two samples from the southern flow lobe is 1.39, disputing the presence of more than one crystal population (Figure 2). Although some chemically heterogeneous feldspars are present in Cerro del Medio rhyolites (Figure 6), sanidine crystals that show no visible evidence of alteration have chemical compositions ranging from $Or_{45}Ab_{53}An_2$ to $Or_{48}Ab_{50}An_2$, significantly different from UBT feldspar [*Phillips et al.*, 2007].

5.4. Excess Argon

[46] A further concern related to the similarity in ages of the UBT, the Deer Canyon and Redondo Creek members, and Cerro del Medio is the possible presence of excess argon ($^{40}Ar_E$), which in significant amounts can cause apparent ^{40}Ar/^{39}Ar ages to be older than eruption ages. *Winick et al.* [2001] identified $^{40}Ar_E$ in melt inclusions in the UBT. *Singer and Brown* [2002] also documented $^{40}Ar_E$ in the Cerro Santa Rosa I dome. *Esser et al.* [1997] found $^{40}Ar_E$ in melt inclusions in zero-age anorthoclase phenocrysts from Erebus volcano, and demonstrated a relationship between Cl/K ratio and apparent age of melt inclusion-bearing anorthoclase crystals, indicating that $^{40}Ar_E$ resides in melt inclusions within Erebus anorthoclase crystals. Many sanidine crystals from the Deer Canyon and Redondo Creek members, and the UBT, contain melt inclusions that are potential hosts for $^{40}Ar_E$.

[47] *Kelley* [2002] suggests treating $^{40}Ar_E$ as an incompatible trace element, which means that Ar strongly partitions from crystals into melts in magmatic systems. Fluids or melts are in effect "infinite reservoirs" for radiogenic argon in most systems. Most K-Ar and ^{40}Ar/^{39}Ar analyses are $^{40}Ar_E$ free and yield true ages because small amounts of $^{40}Ar_E$, if present, would usually be overwhelmed by in situ radiogenic argon when the crystals cooled below their

closure temperatures. However, silicic magmas can contain elevated levels of ^{40}Ar that are derived from older surrounding wall rocks [*Draper and Carroll*, 1995]. When crystals form in the magma chamber, they sometimes trap inclusions of melt. Several studies have investigated the nature of these trapped melt inclusions in quartz. Initial interpretations indicated that ^{40}Ar in melt inclusion-bearing quartz is derived from the in situ decay of ^{40}K at magmatic temperatures and that once crystallized, quartz is a closed system to the diffusion of Ar [*van den Bogaard and Schirnick*, 1995]. Subsequent studies have shown that melt inclusion-bearing quartz is nonretentive of Ar at magmatic temperatures and therefore should be in equilibrium with the surrounding melt at the time of eruption [*Boyce et al.*, 1999; *Winick et al.*, 2001], indicating that the ^{40}Ar found in melt inclusions is not radiogenic argon, but is $^{40}Ar_E$. Upon eruption, rapid cooling of the crystals inhibits the diffusive escape of $^{40}Ar_E$.

[48] We carried out two tests to investigate the presence and abundance $^{40}Ar_E$ in the UBT and the Deer Canyon Member. The first test utilized methods similar to those employed by *Winick et al.* [2001], in which we identified $^{40}Ar_E$ in melt inclusion-bearing quartz and calculated its effect on the ^{40}Ar/^{39}Ar age of sanidine phenocrysts. Comparison of comagmatic quartz and sanidine is appropriate because they have similar Ar diffusion characteristics [*Boyce et al.*, 1999; *McDougall and Harrison*, 1999]. The ^{40}Ar/^{39}Ar integrated ages of step heated melt inclusion-bearing quartz from UBT sample EP-44 and Deer Canyon tuff sample EP-31 (5.66 ± 0.43 Ma and 35.2 ± 2.4 Ma, respectively) are significantly older than the known eruption ages for both of these units (Table 3). Using the estimated abundance of melt inclusions in sanidine (from electron microprobe images), the concentration of $^{40}Ar_E$ in melt inclusions (from ^{40}Ar/^{39}Ar analysis of melt inclusion-bearing quartz), and the eruption age (from ^{40}Ar/^{39}Ar single-crystal sanidine analysis), it is estimated that $^{40}Ar_E$ in melt inclusions could increase the ^{40}Ar/^{39}Ar apparent age of sanidine by 4.2 ka for the UBT and 3.6 ka for the Deer Canyon Member [*Phillips*, 2004]. *Winick et al.* [2001] estimated that $^{40}Ar_E$ bearing melt inclusions in the UBT Plinian deposit could increase the apparent age of sanidine by as much as 38 ka. Three main variables contribute to the difference in results between the two studies: *Winick et al.* [2001] (1) calculated a higher concentration of $^{40}Ar_E$ in melt inclusions, which is the result of using an older measured age for melt inclusion-bearing quartz, (2) measured a higher concentration of melt inclusions in sanidine, and (3) investigated the rapidly cooled UBT Plinian deposit, whereas we studied the UBT ignimbrite deposit, in which sanidine crystals would have been exposed to elevated temperatures for longer than those in the Plinian deposits, promoting the degassing of $^{40}Ar_E$ from trapped melt inclusions.

[49] Our calculated values of 4.2 ka and 3.6 ka are much smaller than the 2σ error on single-crystal laser fusion or step heating analyses of sanidine from EP-44 and EP-31, indicating that $^{40}Ar_E$ in melt inclusions should not have a measurable effect on the ^{40}Ar/^{39}Ar ages of sanidine from the UBT or the Deer Canyon Member.

[50] In the second test, we measured $^{40}Ar_E$ in crushed and HF etched sanidine. The sample preparation procedure for this experiment, similar to that used by *Esser et al.* [1997], was designed to remove melt inclusions from sanidine phenocrysts and therefore remove or decrease $^{40}Ar_E$ that may reside in these inclusions. The "surface etched" splits were separated prior to HF etching and should have retained any trapped melt inclusions that were present. Electron microprobe images of sanidine from EP-44 (UBT) reveal trapped melt inclusions as large as 200 μm and the proportion of melt inclusions to crystal in sanidine was estimated at 0.19%. Because sanidine phenocrysts were crushed to 90–125 μm before etching, at least some of the trapped melt inclusions were etched by HF and removed from the "crushed and etched" split. In portions of the splits from EP-31 (Deer Canyon tuff), one small melt inclusion (<50 μm) was documented in the "surface etched" split and no melt inclusions were found in the "crushed and etched" split. The abundance of melt inclusions in sanidine from this sample was estimated at 0.02%. Neither sample shows significant differences in age between the "surface etched" and the "crushed and etched" splits (Figure 3 and Table 4). This finding implies that significant $^{40}Ar_E$ does not reside in melt inclusions in sanidine. Although the ages of EP-44 and EP-31 are not affected by HF etching, the radiogenic yields are substantially higher in the "crushed and etched" splits than in the "surface etched" splits, which is apparently due to the removal of $^{40}Ar_{atm}$ in trapped melt inclusions by HF etching.

[51] The age spectra in Figure 3 are flat, indicating a homogeneous distribution of radiogenic ^{40}Ar in each sample and a lack of heterogeneously distributed $^{40}Ar_E$ in melt inclusions, which can disturb age spectra [*Esser et al.*, 1997]. Although the possibility exists that $^{40}Ar_E$ is homogeneously distributed in crystal lattices, isochrons from single-crystal analyses of sanidine for EP-44 and EP-31 show that ^{40}Ar/^{36}Ar ratios are indistinguishable from the atmospheric value (295.5), implying that measurable $^{40}Ar_E$ is not present in these samples [*McDougall and Harrison*, 1999]. In contrast, *Singer and Brown* [2002] identified $^{40}Ar_E$ in the Cerro Santa Rosa I dome by an elevated ^{40}Ar/^{36}Ar isochron intercept and by a saddle shaped incremental heating age spectrum. It has been shown that ring fracture domes were erupted from multiple temporally and spatially separated magma chambers and not from a single long-lived UBT magma chamber [*Spell et al.*, 1993] and therefore magma processes and the incorporation of $^{40}Ar_E$ could have differed considerably between Cerro Santa Rosa I and the earlier UBT and Deer Canyon eruptions. We did not employ our test for excess argon for Cerro del Medio because feldspars did not contain melt inclusions, However, isochrons from both Cerro del Medio samples used to calculate the pooled age of 1.229 ± 0.017 Ma exhibit ^{40}Ar/^{36}Ar ratios indistinguishable from the atmospheric value of 295.5 (298 ± 19; 300 ± 17), possibly implying that Cerro del Medio tapped a different magma reservoir than Cerro Santa Rosa I.

[52] In summary, the results of both of our tests show that $^{40}Ar_E$ is not present in sufficient amounts to affect the ^{40}Ar/^{39}Ar age of sanidine from the UBT or the Deer Canyon Member.

6. Summary and Conclusions

[53] 1. The UBT and Cerro del Medio are the lower and upper constraints on the timing of resurgence and yield

^{40}Ar/^{39}Ar ages of 1.256 ± 0.010 Ma and 1.229 ± 0.017 Ma, respectively. This leaves 27 ± 27 ka for the duration of resurgent uplift. Taking into consideration the relief of the resurgent dome from the surrounding caldera floor, the resurgent dome was probably uplifted at a minimum rate of 1.9 cm/yr.

[54] 2. The Deer Canyon and Redondo Creek members of the Valles Rhyolite Formation overlie UBT and are intricately interlayered with earliest caldera fill sediments. The ^{40}Ar/^{39}Ar ages for the Deer Canyon Member range from 1.229 ± 0.013 Ma to 1.283 ± 0.017 Ma, and ages for the Redondo Creek Member range from 1.208 ± 0.017 Ma to 1.239 ± 0.017 Ma. One sample from each unit is significantly younger than the UBT, whereas the other 10 samples yield ages indistinguishable from the UBT. These results indicate that both units might have started to erupt soon after caldera collapse and continued to erupt later in the postcollapse history.

[55] 3. Results from ^{40}Ar/^{39}Ar analysis of melt inclusion-bearing quartz and crushed and HF-etched sanidine show that excess argon in melt inclusions does not have a measurable effect on the ^{40}Ar/^{39}Ar age of sanidine phenocrysts from the UBT or the Deer Canyon Member.

[56] **Acknowledgments.** This work was supported by the New Mexico Bureau of Geology and Mineral Resources (NMBGMR), the New Mexico Geological Society, the Colorado Scientific Society, and the New Mexico Tech Graduate Student Association. E.P. was funded by a fellowship from the New Mexico Institute of Mining and Technology Graduate Office. F.G. was funded by Los Alamos National Laboratory (2001–2003) and by the State Map Program of NMBGMR (2004–2006). We extend our thanks to Lisa Peters, Rich Esser, and Matt Heizler for helpful discussions concerning ^{40}Ar/^{39}Ar data. We also thank Dennis Trujillo and Bob Parmenter (Valles caldera National Preserve) for access and logistical support during this project and Joel Bensing for his field assistance. Constructive reviews by Brad Singer, Alan Deino, and Robert Duncan are gratefully acknowledged.

References

Bailey, R. A., R. L. Smith, and C. S. Ross (1969), Stratigraphic nomenclature of volcanic rocks in the Jemez Mountains, New Mexico, *U.S. Geol. Surv. Bull.*, *1274-P*, 1–19.

Baldridge, W. S., P. E. Damon, M. Shafiqullah, and R. J. Bridwell (1980), Evolution of the central Rio Grande Rift, New Mexico: New potassium-argon ages, *Earth Planet. Sci. Lett.*, *51*, 309–321.

Baldridge, W. S., Y. Bartov, and A. Kron (1983), Geologic map of the Rio Grande Rift and southeastern Colorado Plateau, New Mexico and Arizona, in *Rio Grande Rift: Tectonics and Magmatism*, edited by R. E. Riecker, supplement, AGU, Washington, D. C.

Boyce, J. W., M. Grove, and M. R. Reid (1999), Experimental evidence for the non-retentive behavior of Ar from melt inclusions in quartz phenocrysts, *Eos Trans. AGU*, *80*(46), Fall Meet. Suppl., Abstract F-1130.

Caress, M. E. (1996), Zonation of alkali feldspar compositions in the Tshirege Member of the Bandelier Tuff: Implications for magma chamber and eruptive processes, *Field Trip Guideb. N. M. Geol. Soc.*, *47*, 275–283.

Chapin, C. E., and W. R. Seager (1975), Evolution of the Rio Grande Rift in the Socorro and Las Cruces area, *Field Trip Guideb. N. M. Geol. Soc.*, *26*, 297–321.

Chen, J. K., F. W. Taylor, R. L. Edwards, H. Cheng, and G. S. Burr (1995), Recent emerged reef terraces of the Yenkahe resurgent block, Tanna, Vanuatu: Implications for volcanic, landslide and tsunami hazards, *J. Geol.*, *103*, 577–590.

Chen, Y., P. E. Smith, N. M. Evensen, D. York, and K. R. Lajoie (1996), The edge of time; dating young volcanic ash layers with the ^{40}Ar-^{39}Ar laser probe, *Science*, *274*, 1176–1178.

Chipera, S. J., F. Goff, C. J. Goff, and M. Fittapaldo (2007), Zeolitization of intracaldera sediments and rhyolitic rocks in the 1.25 Ma lake of Valles caldera, New Mexico, U.S.A., *J. Volcanol. Geotherm. Res.*, in press.

Dalrymple, G. B., and M. A. Lanphere (1969), *Potassium-Argon Dating; Principles, Techniques and Applications to Geochronology*, 258 pp., W. H. Freeman, San Francisco, Calif.

Deino, A., and R. Potts (1990), Single-crystal ^{40}Ar/^{39}Ar dating of the Olorgesailie Formation, southern Kenya Rift, *J. Geophys. Res.*, *95*, 8453–8470.

Deino, A., and R. Potts (1992), Age-probability spectra for examination of single-crystal ^{40}Ar/^{39}Ar dating results: Examples form Olorgesailie, southern Kenya Rift, *Quat. Int.*, *13/14*, 47–53.

Doell, R. R., G. B. Dalrymple, R. L. Smith, and R. A. Bailey (1968), Paleomagnetism, potassium-argon ages, and geology of rhyolites and associated rocks of the Valles caldera, New Mexico, *Mem. Geol. Soc. Am.*, *116*, 211–248.

Draper, D. S., and M. R. Carroll (1995), Argon diffusion and solubility in silicic glasses exposed to an Ar-He gas mixture, *Earth Planet. Sci. Lett.*, *132*, 15–24.

Dzurisin, D., C. Wicks, and W. Thatcher (1999), Renewed uplift at the Yellowstone Caldera measured by leveling surveys and satellite radar interferometry, *Bull. Volcanol.*, *61*, 349–355.

Esser, R. P., W. C. McIntosh, M. T. Heizler, and P. R. Kyle (1997), Excess argon in melt inclusions in zero-age anorthoclase feldspar from Mt. Erebus, Antarctica, as revealed by the ^{40}Ar/^{39}Ar method, *Geochim. Cosmochim. Acta*, *61*, 3789–3801.

Fisher, R. V., G. Heiken, and J. B. Hulen (1997), *Volcanoes; Crucibles of Change*, 317 pp., Princeton Univ. Press, Princeton, N. J.

Gansecki, C. A., G. A. Mahood, and M. O. McWilliams (1996), ^{40}Ar/^{39}Ar geochronology of rhyolites erupted following collapse of the Yellowstone Caldera, Yellowstone Plateau volcanic field: Implications for crustal contamination, *Earth Planet. Sci. Lett.*, *142*, 91–108.

Gardner, J. N., and F. Goff (1984), Potassium-argon dates from the Jemez volcanic field; implications for tectonic activity in the north-central Rio Grande Rift, *Field Trip Guideb. N. M. Geol. Soc.*, *35*, 75–81.

Gardner, J. N., F. Goff, S. Garcia, and R. C. Hagan (1986), Stratigraphic relations and lithologic variations in the Jemez volcanic field, New Mexico, *J. Geophys. Res.*, *91*, 1763–1778.

Gardner, J. N., F. Goff, S. L. Reneau, M. M. Sandoval, P. G. Drakos, D. Katzman, and C. J. Goff (2006), Preliminary geologic map of the Valle Toledo quadrangle, Los Alamos and Sandoval counties, New Mexico, *Geol. Map OF-GM-133*, scale 1:24,000, N. M. Bur. of Geol. and Miner. Resour., Socorro.

Goff, F., and J. N. Gardner (2004), Late Cenozoic geochronology of volcanism and mineralization in the Jemez Mountains and Valles caldera, north central New Mexico, in *The Geology of New Mexico, A Geologic History*, edited by G. Mack and K. Giles, *N. M. Geol. Soc. Spec. Publ. 11*, 295–312.

Goff, F., S. L. Reneau, S. Lynch, C. J. Goff, J. N. Gardner, P. Drakos, and D. Katzman (2005), Preliminary geologic map of the Bland 7.5-minute quadrangle, Los Alamos and Sandoval Counties, New Mexico, *Open File Geol. Map OF-GM 112*, scale 1:24,000, N. M. Bur. of Geol. and Miner. Resour., Socorro.

Goff, F., J. N. Gardner, S. L. Reneau, and C. J. Goff (2006a), Preliminary geologic map of the Redondo Peak quadrangle, Sandoval County, New Mexico, *Open File Geol. Map OF-GM 111*, scale 1:24,000, N. M. Bur. of Geol. and Miner. Resour., Socorro.

Goff, F., S. L. Reneau, C. J. Goff, and J. N. Gardner (2006b), Preliminary geologic map of the Valle San Antonio quadrangle, Sandoval County, New Mexico, *Open File Geol. Map OF-GM 132*, scale 1:24,000, N. M. Bur. of Geol. and Miner. Resour., Socorro.

Heiken, G., F. Goff, J. Stix, S. Tamanyu, M. Shafiqullah, S. Garcia, and R. Hagen (1986), Intracaldera Volcanic Activity, Toledo Caldera And Embayment, Jemez Mountains, New-Mexico, *J. Geophys. Res.*, *91*, 1799–1815.

Hu, Q., P. E. Smith, N. M. Evensen, and D. York (1994), Lasing in the Holocene; extending the ^{40}Ar-^{39}Ar laser probe method into the ^{14}C age range, *Earth Planet. Sci. Lett.*, *123*, 331–336.

Izett, G. A., and J. D. Obradovich (1994), The ^{40}Ar/^{39}Ar age constraints for the Jaramillo normal subchron and the Matuyama-Bruhnes geomagnetic boundary, *J. Geophys. Res.*, *99*, 2925–2934.

Jackson, S. M., R. B. Smith, and T. L. Olsen (1984), Recent uplift of the Yellowstone Caldera from precision gravity measurements, *Eos Trans. AGU*, *65*, 1118.

Kaizuka, S., C. G. Newhall, N. Oyagi, and H. Yagi (1989), Remarkable unrest of Iwo-Jima Caldera, in *Continental Magmatism Abstracts*, *General Assembly of the International Association of Volcanology and Chemistry of the Earth's Interior*, *N. M. Bur. Geol. Miner. Resour. Bull.*, *131*, 146.

Kelley, S. (2002), Excess argon in K-Ar and Ar-Ar geochronology, *Chem. Geol.*, *188*(1–2), 1–22, doi:10.1016/S0009-2541 (02)00064-5.

Lanphere, M. A., and H. Baadsgaard (2001), Precise K-Ar, ^{40}Ar/^{39}Ar, Rb-Sr and U/Pb mineral ages from the 27.5 Ma Fish Canyon Tuff reference standard, *Chem. Geol.*, *175*, 653–671.

Lipman, P. W. (1976), Caldera-collapse breccias in the western San Juan Mountains, Colorado, *Geol. Soc. Am. Bull.*, *87*, 1397–1410.

Luongo, G., E. Cubellis, F. Obrizzo, and S. M. Petrazzuoli (1991), The mechanics of the Campi Flegrei resurgent caldera; a model, *J. Volcanol. Geotherm. Res.*, *45*, 161–172.

Marvin, R. F., and S. W. Dobson (1979), Radiometric ages; compilation B, U.S. Geological Survey, *Isochron West*, *26*, 3–30.

McDougall, I., and T. M. Harrison (Eds.) (1999), *Geochronology and Thermochronology by the ^{40}Ar/^{39}Ar Method*, 2nd ed., 269 pp., Oxford Univ. Press, New York.

Nielson, D. L., and J. B. Hulen (1984), Internal geology and evolution of the Redondo Dome, Valles caldera, New Mexico, *J. Geophys. Res.*, *89*, 8695–8711.

Olsen, K. H., W. S. Baldridge, and J. F. Callender (1987), Rio Grande Rift; an overview, *Tectonophysics*, *143*, 119–139.

Orsi, G., L. Civetta, C. Del Gaudio, S. de Vita, M. A. Di Vito, R. Isaia, S. M. Petrazzuoli, G. P. Ricciardi, and C. Ricco (1999), Short-term ground deformations and seismicity in the resurgent Campi Flegrei Caldera (Italy): An example of active block-resurgence in a densely populated area, *J. Volcanol. Geotherm. Res.*, *91*, 415–451.

Pelton, J. R., and R. B. Smith (1979), Recent crustal uplift in Yellowstone National Park, *Science*, *206*, 1179–1182.

Phillips, E. H. (2004), Collapse and Resurgence of the Valles caldera, Jemez Mountains, New Mexico: ^{40}Ar/^{39}Ar age constraints on the timing and duration of resurgence and ages of megabreccia blocks, M. S. thesis, 200 pp, N. M. Inst. of Min. and Technol., Socorro.

Phillips, E. H., F. Goff, P. R. Kyle, W. C. McIntosh, N. W. Dunbar, and J. N. Gardner (2007), Data repository for "^{40}Ar/^{39}Ar age constraints on the duration of resurgence at the Valles caldera, New Mexico, *Open File Rep. OF-AR-26*, N. M. Bur. of Geol. and Miner. Resour., Socorro. (Available at http://geoinfo.nmt.edu/publications/openfile/argon/home.html)

Renne, P. R., C. C. Swisher, A. L. Deino, D. B. Karner, T. L. Owens, and D. J. DePaolo (1998), Intercalibration of standards, absolute ages and uncertainties in ^{40}Ar/^{39}Ar dating, *Chem. Geol.*, *145*, 117–152.

Savage, J. C., and M. M. Clark (1982), Magmatic resurgence in Long Valley Caldera, California; possible cause of the 1980 Mammoth Lakes earthquakes, *Science*, *217*, 531–533.

Seager, W. R., M. Shafiqullah, J. W. Hawley, and R. F. Marvin (1984), New K-Ar dates from basalts and the evolution of the southern Rio Grande Rift, *Geol. Soc. Am. Bull.*, *95*, 89–99.

Self, S., F. Goff, J. N. Gardner, J. V. Wright, and W. M. Kite (1986), Explosive rhyolitic volcanism in the Jemez Mountains: Vent locations, caldera development and relation to regional structure, *J. Geophys. Res.*, *91*, 1779–1798.

Self, S., G. Heiken, M. L. Sykes, K. Wohletz, R. V. Fisher, and D. P. Dethier (1996), Field excursions to the Jemez Mountains, New Mexico, *N. M. Bur. Mines Miner. Resour. Bull.*, *134*, 72 pp.

Singer, B., and L. L. Brown (2002), The Santa Rosa event: ^{40}Ar/^{39}Ar and paleomagnetic results from the Valles rhyolite near Jaramillo Creek, Jemez Mountains, New Mexico, *Earth Planet. Sci. Lett.*, *197*, 51–64.

Smith, R. B., and L. W. Braile (1994), The Yellowstone Hotspot, *J. Volcanol. Geotherm. Res.*, *61*, 121–187.

Smith, R. L., and R. A. Bailey (1968), Resurgent cauldrons, *Mem. Geol. Soc. Am.*, *116*, 613–662.

Smith, R. L., R. A. Bailey, and C. S. Ross (1970), Geologic map of the Jemez Mountains, New Mexico, *U.S. Geol. Surv. Misc. Invest. Map*, *I-571*.

Sorey, M. L., V. S. McConnell, and E. Roeloffs (2003), Summary of recent research in Long Valley caldera, California, *J. Volcanol. Geotherm. Res.*, *127*(3–4), 165–173, doi:10.1016/S0377-0273 (03)00168-9.

Spell, T. L., and T. M. Harrison (1993), ^{40}Ar/^{39}Ar geochronology of post-Valles caldera rhyolites, Jemez Volcanic Field, New Mexico, *J. Geophys. Res.*, *98*, 8031–8051.

Spell, T. L., P. R. Kyle, M. F. Thirlwall, and A. R. Campbell (1993), Isotopic and Geochemical Constraints on the Origin and Evolution of Postcollapse Rhyolites in the Valles caldera, New Mexico, *J. Geophys. Res.*, *98*, 19,723–19,739.

Spell, T. L., I. McDougall, and A. P. Doulgeris (1996), Cerro Toledo rhyolite, Jemez Volcanic Field, New Mexico: ^{40}Ar/^{39}Ar geochronology of eruptions between two caldera-forming events, *Geol. Soc. Am. Bull.*, *108*, 1549–1556.

Spell, T. L., E. I. Smith, A. Sanford, and K. A. Zanetti (2001), Systematics of xenocrystic contamination; preservation of discrete feldspar populations at McCullough Pass Caldera revealed by ^{40}Ar/^{39}Ar Ar dating, *Earth Planet. Sci. Lett.*, *190*, 153–165.

Steiger, R. H., and E. Jäger (1977), Subcommission on geochronology: Convention on the use of decay constants in geo- and cosmochronology, *Earth Planet. Sci. Lett.*, *36*, 359–362.

Stix, J., F. Goff, M. P. Gorton, G. Heiken, and S. R. Garcia (1988), Restoration of compositional zonation in the Bandelier silicic magma chamber between two caldera-forming eruptions: Geochemistry and origin of the Cerro Toledo rhyolite, Jemez Mountains, New Mexico, *J. Geophys. Res.*, *93*, 6129–6147.

Taylor, J. R. (1982), *An Introduction to Error Analysis: The Study of Uncertainties in Physical Measurements*, 270 pp., Univ. Sci. Books, Mill Valley, Calif.

van den Bogaard, P., and C. Schirnick (1995), ^{40}Ar/^{39}Ar laser probe ages of Bishop Tuff quartz phenocrysts substantiate long-lived silicic magma chamber at Long Valley, United States, *Geology*, *23*, 759–762.

Winick, J. A., W. C. McIntosh, and N. W. Dunbar (2001), Melt-inclusion-hosted excess argon ^{40}Ar in the quartz crystals of the Bishop and Bandelier magma systems, *Geology*, *29*, 275–278.

N. W. Dunbar, New Mexico Bureau of Geology and Mineral Resources, New Mexico Institute of Mining and Technology, Socorro, NM 87801, USA.

J. N. Gardner, Earth and Environmental Sciences Division, Los Alamos National Laboratory, Los Alamos, NM 87545, USA.

F. Goff, Department of Earth and Planetary Sciences, University of New Mexico, Albuquerque, NM 87131, USA.

P. R. Kyle, W. C. McIntosh, and E. H. Phillips, Department of Earth and Environmental Science, New Mexico Institute of Mining and Technology, Socorro, NM 87801, USA.